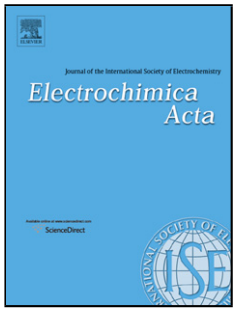

Title: Electrochemical impedance spectroscopy analysis of A-beta (1-42) peptide using a nanostructured biochip

Author: Chia-Che Wu Bien-Chen Ku Chien-Hsien Ko Chun-Che Chiu Gou-Jen Wang Yuan-Han Yang Shyh-Jong Wu

PII: S0013-4686(14)00892-5
DOI: http://dx.doi.org/doi:10.1016/j.electacta.2014.04.132
Reference: EA 22638

To appear in: *Electrochimica Acta*

Received date: 18-12-2013
Revised date: 22-4-2014
Accepted date: 23-4-2014

Please cite this article as: C.-C. Wu, B.-C. Ku, C.-H. Ko, C.-C. Chiu, G.-J. Wang, Y.-H. Yang, S.-J. Wu, Electrochemical impedance spectroscopy analysis of A-beta (1-42) peptide using a nanostructured biochip, *Electrochimica Acta* (2014), http://dx.doi.org/10.1016/j.electacta.2014.04.132

Electrochemical impedance spectroscopy analysis of A-beta (1-42) peptide using a nanostructured biochip

Chia-Che Wu[a]*, Bien-Chen Ku[b], Chien-Hsien Ko[b], Chun-Che Chiu[b], Gou-Jen Wang[b,c], Yuan-Han Yang[d,e], Shyh-Jong Wu[f]

[a, b] Department of Mechanical Engineering, National Chung Hsing University, 250, Taichung, 402, Taiwan

[c] Graduate Institute of Biomedical Engineering, National Chung Hsing University, 250, Taichung, 402, Taiwan

[d] Department of and Master's Program in Neurology, Faculty of Medicine, Kaohsiung Medical University, Kaohsiung, 807, Taiwan

[e] Department of Neurology, Kaohsiung Municipal Ta-Tung Hospital, Kaohsiung, 807, Taiwan

[e] Department of Medical Laboratory Science and Biotechnology, Kaohsiung Medical University, Kaohsiung, 807, Taiwan

Submitted to

Journal of the ELECTROCHIMICA ACTA

[a] Corresponding author: Tel: +886–4–22840433 ext 405; Fax: +886–4–22877170;
E-mail: josephwu@dragon.nchu.edu.tw
Department of Mechanical Engineering, National Chung Hsing University, Taichung, 402, Taiwan, 402

Abstract

A-beta (1-42) peptide (Aβ (1-42)) is a potential candidate for the prediction of Alzheimer's disease. In this study, we demonstrate a nanostructured biosensor based on electrochemical impedance spectroscopy (EIS) with uniformly deposited gold nanoparticles (GNPs) as the sensing electrode for effective detection of Aβ (1-42). An anodic aluminum oxide (AAO) layer with a nanohemisphere array was used as the substrate. A gold thin film was sputtered onto the AAO substrate to serve as the electrode for GNP deposition and the sensor for Aβ (1-42). Aβ (1-42) antibody was prepared, and its specificity with Aβ (1-42) was verified by Western blot. We observed aggregation of Aβ (1-42) at 1 μg ml^{-1}. The morphology of Aβ (1-42) was in the form of round aggregates with diameter of around 1500–2000 nm. EIS measurements for nanostructured biosensors were used to determine the concentration of Aβ (1-42). The plot for the dependence of EIS concentration measurement resulted in an equation$\Delta Rct = 29098*\log [A\beta (1\text{-}42)] + 90150$ with an R^2 value of 0.9916. The linear detection range was between 1 pg ml^{-1} and 10 ng ml^{-1} of Aβ (1-42).

Keywords: electrochemical impedance spectroscopy (EIS); anodic aluminum oxide (AAO); A-beta (1-42) peptide; Alzheimer disease (AD); nanostructured biosensor

1. Introduction

Alzheimer's disease (AD) is the sixth leading cause of death in the United States, and its progression cannot be prevented, cured, or slowed. AD is thought to be caused by the accumulation of insoluble fibrils, also known as amyloid plaque, in the brain. The major component of amyloid plaque exists in two primary forms: A-beta (1-40) peptide (Aβ (1-40)) and A-beta (1-42) peptide (Aβ (1-42)) [1]. These peptides [2] are produced by processing a larger amyloid precursor protein [3], resulting from sequential cleavage by two proteases, named β- and γ-secretases [4-6] and differ in the absence or presence of two extra C-terminal residues. The formation of senile plaques in the brain tissues consisting of Aβ (1-42) aggregates is considered a major pathological hallmark of AD. A recent report [7-9] showed that Aβ (1-42) is more hydrophobic, aggregates more easily, and is present at higher concentrations in the plaques of AD individuals than Aβ (1-40). Thus, monitoring Aβ (1-42) [10,11] concentration may be a suitable candidate to predict AD. Niels Andreasen et al. [12] found decreased levels of Aβ (1-42) in cerebrospinal fluid (CSF) of probable and possible AD individuals. Two CSF pools were used as internal controls: a normal CSF pool sample from patients with psychiatric or minor neurological disorders with a mean Aβ (1-42) value of 700 pg ml^{-1}, and an AD pool with a mean Aβ (1-42) level of 383 pg ml^{-1}. To diagnose probable cases of AD prior to onset, the plasma concentration of Aβ (1-42) from patients should also be monitored. It was demonstrated by Pankaj D. Mehta et al. [13] that Aβ (1-42) levels in plasma in patients with AD and controls could be detected from 25 to 85 pg ml^{-1}.

A few attempts have been made in the past to develop new assay methods for screening Aβ (1-42). These methods include capillary electrophoresis [14], mass spectrometry [15], enzyme-linked immunosorbent assay [16], surface plasma

resonance spectrometry [17], scanning tunneling microscopy [18], surface-enhanced Raman spectroscopy [19], cell-based assays [20], quartz crystal microbalance [21] and fluorescence-based methods [22]. Most of these methods are time consuming, expensive, labor intensive, and require months or years to complete.

Since electrochemistry is known to be a cost-effective method to construct biosensors because of its high sensitivity, reliability, and convenience, more studies on the development of electrochemical peptide-based biosensors should be conducted [23]. Electrochemical impedance spectroscopy (EIS) detection, which is a label-free process, has enabled simplification of detection and enhancement of measurement sensitivity [22-25]. The EIS method [26] measures the impedance of an electrode—solution interface by applying a small sinusoidal applied potential difference at a particular frequency to the interface. The impedance of the electrode–solution interface changes when the target analyte is immobilized on the probe. Therefore, the concentration of the target analyte can be detected in relation to the impedance variations.

Meijia Wang et al. [27] used colloidal Au to enhance the amount of antibody immobilized on a gold electrode and ultimately monitored the interaction of antigen–antibody by impedance measurement. Kagan Kerman et al. [28] presented the first electrochemical detection, characterization, and kinetic study of the aggregation of Aβ (1-42) using three different voltammetric techniques at a glassy carbon electrode. Kagan Kerman et al. [29] demonstrated the application of gold nanoparticles (GNPs) in the electrochemical detection of protein phosphorylation. Immobilization of Aβ (1-40) peptide on Au-colloid-modified gold electrodes was developed by Iwona Szymanska [30]. The electrochemical sensing of saccharide–protein interactions using a couple of sialic acid derivatives and

Alzheimer's Aβ (1-42) was described by Miyuki Chikae et al. [31]. Kamrul Islam et al. [2] proposed a simple microfluidic biosensor to analyze very small quantities of Aβ (1-42) on gold surfaces that were modified with GNPs onto the thiol groups of self-assembled 1.6-hexandithiol cross-linkers. On the basis of oligopeptide, a novel strategy to fabricate an electrochemical biosensor is proposed in this study by fine-tuning the scan pulse frequency of square wave voltammetry to synchronize with the surface electron transfer (ET) of the oligopeptide modified on an electrode surface was developed by Hao Li et al. [32].

The challenges to detect Aβ (1-42) in plasma is how to reduce the detection limit down to 10 pg ml^{-1} since Aβ (1-42) levels in plasma in patients with AD and controls were detected from 25 to 85 pg ml^{-1}. The sensitivity of a biosensor relies on the amount of analytes that can be attached on the sensor's electrode. Recent advancements in micro/nano technologies have enhanced the attachment operation [33,34]. Nanomaterials provide a substantially large surface area than that of bulk material or thin film and have been used to magnify the detection signal of biomedical devices [24,35]. Tsai et al. [35] used the barrier layer of anodic aluminum oxide (AAO) film as the template and deposited gold film and gold nanoparticles (GNP) as the electrodes to detect dust mite antigen Der p2. The detection limit of the 3D gold nanoparticle-based biosensor was examined by electrochemical impedance spectroscopy analysis and found to be 1 pg ml^{-1}. Chen et al. [36] developed an electrochemical impedimetric biosensor based on nanostructured polycarbonate substrate and 3D GNP electrode. The detection limit to detect the dust mite antigen was down to 0.1 pg ml^{-1}. Liu et al. [37] used AAO/Au thin film/ GNP electrodes to detect the Immunoglobulin E (IgE) in the serum of an asthma patient. Chin et al. [38] reported detection of mutations to the MD-2 gene promoter using a nanostructured

biosensor with a sensing electrode of gold nanoparticles (GNPs) on a nanohemisphere array.

In this study, we demonstrate an EIS-based nanostructured biosensor, with uniformly deposited GNPs as the sensing electrode for the effective detection of Aβ (1-42). In this device, an anodic aluminum oxide (AAO) layer with a nanohemisphere array was used as the substrate. A gold thin film was sputtered onto the AAO substrate for serving as the electrode for GNP deposition and sensing Aβ (1-42). Aβ (1-42) antibody was prepared, and its specificity was verified with Aβ (1-42) by Western blot. We observed the aggregation of Aβ (1-42) on the nanostructured biosensor surface. An EIS analysis was implemented to measure the concentration of Aβ (1-42).

2. Experimental

2.1. Nanostructured impedance biosensor fabrication

The nanostructured impedance biosensor for the detection of Aβ (1-42) is schematically illustrated in Figure 1. The barrier layer surface of an AAO membrane was adopted as the substrate. A gold thin film was sputtered onto the substrate, followed by uniform electrochemical deposition of GNPs on the gold thin film.

The fabrication details of the nanostructured biosensor are similar to those of previously reported [35] and are concisely depicted below. An AAO membrane was prepared using the conventional anodization process. A honeycomb-like surface barrier layer, containing convex honeycombs of around 80 nm in diameter, was obtained after removing the remaining aluminum from under the barrier layer. The shape of the honeycombs on the barrier layer surface was further modified with 30 wt% phosphoric acid. An electrode consisting of a 10 nm Au thin film was sputtered onto the modified barrier layer surface using a radio frequency magnetron sputter. To

make certain that the sensing area of each biosensor was consistent, a ϕ = 5.5 mm hole was punched into the center of a 2.5 × 2.5 cm^2 piece of parafilm. The bottom surface of the parafilm square was coated with a thin layer of AB glue, and the parafilm was adhered to the Au film barrier layer surface. Finally, a GNP layer was synthesized on the Au thin film by electrochemical deposition.

2.2. Chemicals

Compounds 11-mercaptoundecanoic acid (MUA) and 2-(N-morpholino) ethanesulfonic acid (MES) were obtained from Sigma-Aldrich. Hydroxysuccinimide (NHS) and 1-ethyl-3-[3-dimethylami-nopropyl] carbodiimide hydrochloride (EDC) were purchased from Acros-Organics. $K_3[Fe(CN)_6]\cdot 3H_2O$ and $K_4[Fe(CN)_6]$ were obtained from SHOWA Inc. 10X Phosphate buffered saline (PBS) buffer was purchased from GeneMark Inc. All the chemicals were used without further purification. Serum coloring agents, protein agents, bovine serum albumin (BSA), and rabbit anti-mouse IgG/FITC were obtained from Sigma-Aldrich. Aβ (1-42) monoclonal antibody (12F4) immunoglobulin G (IgG) was obtained from NOVUS Inc. Aβ (1-42) antigen was purchased from Abcam Inc. Aβ (1-42) antigen is an E. coli-expressed recombinant Aβ (1-42) protein; thus, it is a monomer. The protein sequence is (H-Asp-Ala-Glu-Phe-Arg-His-Asp-Ser-Gly-Tyr-Glu-Val-His-His-Gln-Lys -Leu-Val-Phe-Phe-Ala-Glu-Asp-Val-Gly-Ser-Asn-Lys-Gly-Ala-Ile-Ile-Gly-Leu-Met-Val-Gly-Gly-Val-Val-Ile-Ala-OH). The protein GST- Aβ (1-42) is attached with GST tag.

2.3. Surface preparation and immobilization of the antibody/antigen

Detection of the Aβ (1-42) was performed to examine the feasibility of the proposed nanostructured biosensor in clinical applications. The procedures for the

immobilization of antigen on the sensor chip are illustrated in Figure 2. (A) Deposition of gold nano particles on the surface of sensing electrode. The surface of the sensing electrode was washed by successively dipping it in acetone, ethanol, and DI water, followed by ultrasonic shaking for 5 min. (B) $10 \times 10^{-3}\ mol\ l^{-1}$ 20µL of a MUA solution was dipped onto the electrode surface. The sensor was washed three times with a 95% ethanol buffer solution. (C) 30 µL of a NHS and EDC solution with a molar ratio of 1:15 ($2 \times 10^{-3}\ mol\ l^{-1}$: $30 \times 10^{-3}\ mol\ l^{-1}$) in $15 \times 10^{-3}\ mol\ l^{-1}$ MES buffer was dipped onto the sensor and incubated for 1 hour. (D) The sensor was washed three times with DI water followed by dripping 30 µL of a (10 µg ml^{-1}) Aβ (1-42) monoclonal antibody IgG solution onto the sensor and then incubating for 30 min. Aβ (1-42) monoclonal antibody 12F4 is reactive to the C-terminus of beta amyloid and is specific for the isoform ending at the 42nd amino acid. (E) The sensor was rinsed three times with a PBS buffer solution. The binding sites of the antigen molecules that did not bond with the MUA membrane were filled using 30 µL of a 7% BSA solution. (F) 30 µL of the A-beta (1-42) peptide solution was incubated onto the sensor for 30 minutes. to ensure thorough binding.

2.4. Electrochemical analysis

An SP-150 potentiostat (Bio-Logic, USA) was implemented for the cyclic voltammetry (CV) and EIS analysis. The EIS analysis was used to distinguish between antibody and antigen through the measurement of impedance differences. The working electrode, counter electrode, and reference electrode were the nanostructured sensor, Pt film, and Ag/AgCl/3M KCl, respectively. A mixture of 5 mM $Fe(CN)_6^{4-}$, 5 mM $Fe(CN)_6^{3-}$, and 0.1 M KCl in 100 mM MES (pH = 6.0) was used as the buffer solution. The applied DC power and AC power were 0 V and 10 mV, respectively. The scanning AC frequency was between 0.02 Hz and 200 kHz.

2.5. Elemental composition analysis

A PHI 5000 VersaProbe (ULVAC-PHI, Japan) X-ray photoelectron spectroscopy (XPS) instrument was used to analyze the elemental compositions of the electrode surface at each stage of immobilization.

3. Results and Discussion

3.1. Western Blot analysis

The Aβ (1-42) peptide was purchased from Abcam Inc. Aβ (1-42) antigen is an E. coli-express ed recombinant Aβ (1-42) protein; thus, it is a monomer. The protein Aβ (1-42) is attached with GST tag. As show in Figure 3, we used western blot analysis to verify that Aβ (1-42) solution from Abcam Inc. A standard consisting of a known amount of synthetic antigen was also extracted into the SDS sample buffer. The migration of molecular size markers is indicated in kilodaltons. Figure 3 showed that the molecular mass of Aβ (1-42) with GST tag is 31 kDa. We also can find a light band around 4.6kDa which was the expression of Aβ (1-42) without GST tag.

3.2. Sensor fabrication

Figure 4 shows the sensor fabrication results as SEM images of the AAO barrier layer and the GNP-deposited hemispheric electrode array. The gold nanoparticels deposited on the orderly hemispheric electrode array were uniformly and compactly deposited. The diameter of the uniformly deposited GNPs shown in Figure 4B was measured to be 10–15 nm. The high surface-to-volume ratio of the proposed nanostructured biosensor allows more antibodies to attach onto the electrode. Compared to the flat gold electrode which used a sodium citrate solution as the stabilizer, AAO/Au/GNP electrode showed uniform distribution and dense deposition. Our previous report [36] proposed that the uniformly propagated electric flux perpendicular to the hemispheric Au thin film pulls the positive charges carrying Au

nanoparticles in the electrolyte. This means that of AAO/Au/GNP can be densely deposited onto the surface without the necessary of any reducing agent and stabilizer.

A cyclic voltammogram trace was used to estimate the effective sensing areas for the adhesion of the analytes. Figure 5A showed the cyclic voltammograms for flat gold electrode, AAO/gold electrode and AAO/Au/GNP electrode in in 5 mM $Fe(CN)_6^{4-}$, 5 mM $Fe(CN)_6^{3-}$ and 0.1 mol dm^{-3} KCl in PBS buffer (pH 7.4). There were three measuring conditions: three electrode configurations (Au working electrode, Ag/AgCl/3M KCl reference electrode, and Pt counter electrode) each with a scan rate of 50 mVs^{-1}. Figure 5B shows the corresponding current versus time for Figure 5A. By integrating the area under the reducing peak in Figure 5B, the total electric charge of the flat Au electrode, AAO/Au thin film electrode and AAO/Au thin film/GNP electrode are 1482.78μC, 2347.04μC and 2796.3μC, respectively. Since a charge of 386μC per centimeter of gold electrode is required to form AuO, the effective area of the flat Au electrode, AAO/Au thin film electrode and AAO/Au thin film/GNP electrode were 3.8414cm^2, 6.0804 cm^2 and 7.2443 cm^2, respectively. The uniformly distributed GNPs on the nanohemisphere enhance the sensing area. The distingulishing feature of our sensor scheme is that both the hemispheres and electrochemically deposited GNP are uniformly distributed which allows more Aβ (1-42) antibody/antigen immobilization on the sensing surface.

3.3. Antibody/antigen immobilization

3.3.1. Elemental composition analysis

In Table 1, we have extracted results from the XPS spectra regarding the atomic percentage of different elements interfering in chemical functionalization in this study: gold, carbon, oxygen, sulfur, and nitrogen. In fact, we can confirm the chemical stability of the grafted alkanethiolate after formation of the MUA self-assembled monolayers (SAMs); the S/Au ratio remains far above the ratio of the untreated

sample. After being modified by EDC/NHS on a MUA linker, the N/Au ratio also remains far above the ratio of the untreated sample. Moreover, the contact angle was measured with uncoated and coated MUA. Functionalization confirms the presence of COOH group: the immobilization of MUA on the surface shows hydrophilic behavior unlike the uncoated surface, which is largely hydrophobic. Combined with the XPS analysis, these results clearly demonstrate the covalent grafting of the immobilization of MUA and EDC/NHS on the prepared surfaces.

3.3.2. Cyclic volyammograms

The cyclic volyammograms of the AAO/Au/GNP electrode was measure (Figure 6) before and after each step of surface modification with MUA, EDC/NHS, IgG, BSA and Aβ (1-42). As expected, $K_3[Fe(CN)_6]/K_4[Fe(CN)_6]$ shows the reversible behavior on a bare Au electrode with the peak cathode current (I_{pc}) at 0.4274 mA. After the covalent attachment of MUA, the shape of the CV changes dramatically. A quasi-reversible voltammogram with a separation of peak potential (ΔE_p) of 407mV was observed for AAO/Au/GNP electrode after modification with MUA. The EDC/NHS treated MUA/GNP/AU/AAO electrode showed an increase in the peak separation of ΔE_p 499mV. This is attributed to repulsive interaction of polyanions of NHS layer formed over the electrode surface with anionic probe $[Fe(CN)_6^{4-}]$ and $[Fe(CN)_6^{3-}]$ at the surface interface. The decreases in the peak separations of ΔE_p 346mV, 302mV and 231mV after the immobilization of Aβ (1-42) antibody, BSA and Aβ (1-42), respectively. This significant change in the CV curve revealed that the Aβ (1-42) antibody/antigens were effectively immobilized on the nanostructured electrode.

3.4. Optimization of antibody immobilization

To optimize Aβ (1-42) antibody immobilization, the original 0.5mg ml^{-1} antibody solution was diluted to 1ng ml^{-1}, 10ng ml^{-1}, 100ng ml^{-1}, 1μg ml^{-1}, and 10μg

ml^{-1}. After immobilization of antibody, EIS was conducted to measure the variation in charge transfer resistance at different antibody concentrations since it is known that EIS is more sensitive than CV in evaluation of SAMs. The frequency ranges for the measurements are 200kHz to 20mHz.

The impedance results have been fit by complex nonlinear least-squares (CNLS) to four equivalent circuits. Impedance measurements are often fit to the Randle equivalent [39], where R_{ct} is the charge transfer resistance, C_d is the differential capacitance, and R_s is the solution-phase resistance. Aβ (1-42) can be most sensitively detected through the increase in the charge transfer resistance with increasing protein concentration, since this causes an increase in the protein film thickness on the electrodes. However, there is an increasing trend to present novel equivalent circuits. Lee et al. [40] propose a modified Randles equivalent electrical circuit including a solution resistance, R_s, a constant phase element, CPE, an electron-transfer resistance, R_{et}, and a Warburg impedance, Z_w. CPE are being frequently used in place of C_d. Instead of an ideal capacitor, the CPE is used to compromise errors due to microscopic roughness and atomic scale inhomogeneity in surfaces. Amirudin et al. [41] presented an equivalent circuit for a polymer-coated metal, where R_u is the uncompensated solution/electrolyte resistance, R_c is the coating pore resistance, C_c is the coating capacitance, C_d is the electrode double-layer capacitance, R_t is the Faradaic charge-transfer resistance and Z_w is the Warburg diffusional impedance.

A drawback in previous circuit model to fit our experimental results is that the physical significance of nano semi-sphere structures and self-assembly layers is not included. To fit our experimental results, the equivalent circuit in Figure 7 was used as the model to represent the nanostructured biosensors in this study, where R_s is the solution resistance, Q_s is the constant phase element between electrodes and

nanostructures, R_{nano} is the nanostructures resistance, R_{ct} denotes the charge transfer resistance, and Q_{ct} is the constant phase element between protein and nanostructures. R_{ct} can be represented by the diameter of the Nyquist plot of the EIS analysis and can be used to indicate the resistance variations due to the antibody bindings. To understand the variations between antibody immobilizations with different concentrations, R_{ct} is considered as an indicator for the evaluation of the optimal antibody concentration on the nanostructured electrode. Figure 8 and Table 3 show various R_{ct} values with respect to corresponding antibody concentrations. It was found that the values of R_{ct} for 1 μg ml^{-1} and 10 μg ml^{-1} diluted antibody solutions were similar. A saturated R_{ct} value was obtained at a concentration of 10 μg ml^{-1}, diluted from the original 0.5 mg ml^{-1} sample. This indicates that this concentration was sufficient to cover the surface of the nanostructured electrode. The concentration of Aβ (1-42) antibody 10 μg ml^{-1} was used in the following experiments.

3.5. Aggregation

Scanning electron microscopy (SEM) and atomic force microscopy (AFM) were used to determine the three-dimensional surface morphologies of nanostructured biosensors after the attachment of Aβ (1-42) and other consecutive layers. The Aβ (1-42) with different concentrations (1 μg ml^{-1}, 10 ng ml^{-1}, 100 pg ml^{-1}, 10 pg ml^{-1}, and 1 pg ml^{-1}) were first applied to the samples and incubated for 30 min. From SEM images, the bare nanostructured biosensor was observed as a smooth semi-sphere with GNPs (Figure 4B). After modification with 1 μg ml^{-1} Aβ (1-42), nanostructured biosensors showed several opaque areas owing to poor conductivity (Figure 10A). In Figure 9B, the morphology of Aβ (1-42) was in the form of round aggregates with a diameter of 1500–2000 nm. AFM images revealed that Aβ (1-42) was in the form of horizontal round aggregates with 1.58–3.83 μm and vertical round aggregates with

152.3-139.4 nm (Figure 10). AFM analysis was performed as described. Briefly, samples containing Aβ (1-42) aggregates were prepared for AFM analysis by spotting a 10 μl of peptide solution onto freshly cleaved mica (Ted Pella). Ashok Parbhu et al. [42] examined the aggregation of freshly prepared Aβ (1-42) and the role of Aβ (1-42) concentration, imaging medium (air, water, or PBS), and agonists/antagonists on Aβ (1-42) fibrillogenesis by AFM. AFM analysis of Aβ (1-42) aggregates after 12 h was reported by Ruitian Liu et al. [43]. Rajinder Bhatia et al. [44] demonstrated that freshly prepared Aβ (1-42) appear as discrete globular aggregates as imaged by AFM. Neurons examined by SEM 24 hour after addition of the Aβ (1-42) exhibited severe surface blebbing [45]. The round-shaped object of Aβ (1-42) is considered to be the self-assembling structure of amyloid-derived diffusible ligands[37]. After modifications with 10 ng ml^{-1}, 100 pg ml^{-1}, 10 pg ml^{-1}, and 1 pg ml^{-1}, few Aβ (1-42) aggregate into round shapes on the nanostructured biosensors. To prevent aggregation, the concentrations of Aβ (1-42) used in the EIS measurement were 10 ng ml^{-1}, 100 pg ml^{-1}, 10 pg ml^{-1}, and 1 pg ml^{-1}.

3.6. Standard curve

In this study, EIS measurements for nanostructured biosensors were used to quantitatively screen the concentration of Aβ (1-42) below 10 ng ml^{-1}. The concentration of Aβ (1-42) antibody 10 μg ml^{-1} was used in the experiments. Each step of Au electrode modification was detected by EIS. The complex impedance is displayed as the sum of the real (Z') and imaginary ($-Z''$) components. The impedance spectrum consisted of a linear part at low frequencies, resulting from the diffusion-limited electrochemical process, and a semicircular portion at high frequencies, corresponding to the ET limited process. The diameter of the semicircle exhibited the ET resistance and blocking effect of the modified layer on the surface.

The changes in its value were associated with the blocking behavior of the peptide layer on the biosensor surface for the redox probe, $[Fe(CN)_6]^{3-/4-}$, which was reflected in the impedance spectra as an increase or a decrease in the diameter of the semicircle at high frequencies. The results extracted from the EIS measurements, which connected with each step of the electrode modification, were in good agreement with those obtained from EIS (Figure 10). The bare gold electrode exhibits small R_{ct} values of the impedance spectra presented as Nyquist plots (Figure 11, curve A). The semicircle in the impedance spectra after the deposition of MUA (Figure 11, curve B) became larger because it acts as an insulating layer on the electrode by introducing a barrier to the interfacial ET. The deposition of EDC/NHS on MUA increased the semicircle diameter, which indicated a higher ET resistance at the electrode interface (Figure 11, curve C). The immobilization of antibody IgG, BSA, and antigen on the biosensor surface were also monitored by EIS. The frequency ranges for the measurements are 200 kHz to 20 mHz.

Table 4 shows the values of the circuit element from the experimental spectra after MUA, EDC/NHS, IgG, BSA and immunoreactions of 100 pg ml^{-1} Aβ(1-42). The statistical values of mean ± standard deviation were calculated in five repetitions. The values of mean error and maximum error for the fitting data simulated by the proposed circuit were 0.78% and 7.82%. The mean error value 0.72% indicated a small difference between the experimental results and simulated data, respectively. In the comparison of solution resistance listed in table 4, R_s kept nearly constant even with different biomolecule modifications on gold nanostructured electrode. The R_s element only represents the solution resistance and not the sum of the solution resistance and the modified layer resistance. The value of Q_s was about four time smaller than the value of Q_{ct}, resulting from a smaller thickness and a larger permittivity of the electrical double layer relative to those of the MUA, EDC/NHS,

IgG, BSA, and Aβ(1-42) layers. R_{ct} was larger than R_{nano} because of the denser structure of the modified layers which stop the electron transfer. Only the value of R_{ct} increased with the MUA, EDC/NHS, IgG, BSA, and Aβ(1-42) modification. Compared to the value of Q_s and Q_{ct}, the capacitive elements showed weak changes. After MUA, EDC/NHS, IgG, BSA, and Aβ(1-42) modification, the values of R_{ct} were 12.8±1.9 kΩ, 34.8±3.6 kΩ, 49.3±2.8 kΩ, 58.1±3.3 kΩ and 646.0±3.7 kΩ, resprctively. R_{ct} can be used to evaluate the binding interaction of nanohemisphere biosensors.

Figure 12 shows the derived calibration plot that corresponds to the ET resistance at the sensing interface with different concentrations of the antigen. The change in ET resistance is calculated as an average of five measurements using the following equation (Table 5):

$$\Delta R_{ct} = R_{ct(Ag)} - R_{ct(Ab)} \quad (1)$$

where $R_{ct(Ag)}$ is the value of the ET resistance after antigen binding to antibody and $R_{ct(Ab)}$ is the value of the ET resistance after the antibody is immobilized on the electrode.

The plot for the dependence of EIS concentration measurement resulted in an equation ΔR_{ct} = 29098*log [Aβ (1-42)] + 90150 with an R^2 value of 0.9916 where [Aβ (1-42)] is the concentration of Aβ (1-42). The linear detection range existed between 1 pg ml^{-1} and 10 ng ml^{-1} of Aβ (1-42). These experimental results were indicative of a successful working model for the detection of Aβ (1-42) on the fabricated biochip. Although the R^2 value for the standard curve obtained is 0.9916, more experiments are required to be repeated to verify the reproducibility of the device. Before the devices can be real clinically implemented, we plan to do the serum detection for both volunteers and AD patients.

The range of linearity (R^2=0.9916) extended from 1 pg ml^{-1} to 10 ng ml^{-1} which is much wider than that reported for the measurement of Aβ (1-42) by ELISA.

Moreover, it is important to remark that the range is adequate for the determination of Aβ (1-42) in clinical samples. The equation described the linear portion in the calibrated is ΔRct = 29098*log [Aβ (1-42)] + 90150. The limit of detection was calculated according to the criterion of ten times the standard deviation (n=5) provided by 1pg ml^{-1} as the noise estimate. The value achieved, 0.01 pg ml^{-1}, was more than 4 orders lower than the lowest values reported for Aβ (1-42) measurement by ELISA (100 pg ml^{-1}, approximately). The distinguishing features of the proposed devices over the reported work can be attributed to four hypotheses. First, the 3D nanostructure of the AAO film could enhance the binding surface of the GNPs. Secondly, the uniformly distribution of the GNPs also enhance the symmetrical distribution of the electrical field intensity. The uniform distribution of the GNPs on the hemisphere array enabled the MUA molecules to attach to individual GNPs, allowing more complete bindings of EDC/NHS molecules and Aβ (1-42). Thirdly, the hemisphere surface allowed the small disturbance of samples that might enhance the binding of Aβ (1-42) antibody and Aβ (1-42). Finally, the electrochemical impedance spectroscopy is more sensitive than enzyme-linked immunosorbent assay such as ELISA and Western Blot. Hence the signals of electrochemical impedance spectroscopy can be greatly enhanced.

3.7. Reproducibility and selectively

The reproducibility of the immunosensor was estimated by determining 100 pg ml^{-1} Aβ (1-42) solutions on different days with different immunosensors prepared for each test. Relative standard deviation value was 1.7% (n=5), therefore demonstrating the reproducibility of the proposed immunosensors. In order to investigate the selectively of the label-free impedimetric immunosensor for Aβ (1-42) detection, the effect of interfering compounds in Aβ (1-42) solution was examined. Aβ (1-42)

solution with the concentration of 100 pg ml^{-1} was passed through a column with Aβ (1-42) antibody 12F4 to remove Aβ (1-42) antigen. The solution was examined by the immunosensor. The EIS results showed that no significant change in the impedimetric responses of R_{et} element. Furthermore, serum from a volunteer was washed by a column with Aβ (1-42) antibody 12F4. Therefore, there was no Aβ (1-42) in the serum. In the EIS measurement, there is no significant change measured by the immunosensor. Then, serum from the same volunteer was also measured by immunosensor. The selectively results provide the high specificity of the immunosensor and its potential to operate in real samples.

The results confirm the proposed nanostructured biosensor with little sample consumptions (25μl), short sample preparation (less than 2 hours) and short detection time (3 minutes) compared to enzyme-linked immunosorbent assay such as ELISA and western blot. In our future works, serums of the AD patients and control group will be collected to establish a complete standard curve for efficient serum detection using the proposed nanostructured biosensors. To enhance the reproducibility and stable of the device, the fabrication of nanostructured plastic substrate using a nickel nanomold by means of hot embossing is going to develop.

4. Conclusion

We have developed a sensitive electrochemical nanostructured biosensor, based on uniformly deposited GNPs as the sensing electrode, for the effective detection of Aβ (1-42). An AAO nanohemisphere array was used as the substrate while deposition of a gold film on the substrate served as the electrode for GNP deposition. Uniformly distributed GNPs on the hemispheric array may increase the surface area of the electrodes so that an increased number of MUA molecules may attach to the electrode, thereby increasing the sequential binding of EDC/NHS and IgG molecules. From the

Western blot, the specificity between Aβ (1-42) and Aβ (1-42) antibody was verified experimentally. EIS measurements for nanostructured biosensors were used to screen the concentration of Aβ (1-42). The plot for the dependence of EIS concentration measurement resulted in an equationΔRct = 29098*log [Aβ (1-42)] + 90150 with an R^2 value of 0.9916. The linear detection range existed between 1 pg ml^{-1} and 10 ng ml^{-1} of Aβ (1-42). The limit of detect of Aβ (1-42) is at least low as 1pg ml^{-1}. This study also demonstrated that the Aβ (1-42) aggregated when the concentration was 1 μg ml^{-1}. The morphology of Aβ (1-42) was in the form of round aggregates having diameter of 1500–2000 nm, determined by SEM and AFM images. The proposed nanostructured biosensor with little sample consumptions (25μl), short sample preparation (less than 2 hours) and short detection time (3 minutes) compared to the measurement of Aβ (1-42) by ELISA and western blot. The nanostructured immunosensors can perform simple and sensitive detections to specifically measure the Aβ (1-42).

Reference

[1]G.B. Stokin, C. Lillo, T.L. Falzone, R.G. Brusch, E. Rockenstein, S.L. Mount, R. Raman, P. Davies, E. Masliah, D.S. Williams, Axonopathy and transport deficits early in the pathogenesis of Alzheimer's disease, Science 307 (2005) 1282.

[2]K. Islam, Y.-C. Jang, R. Chand, S.K. Jha, H.H. Lee, Y.-S. Kim, Microfluidic Biosensor for-Amyloid (1-42) Detection Using Cyclic Voltammetry, J Nanosci Nanotechnol. 11 (2011) 5657.

[3]J. Hardy, Amyloid, the presenilins and Alzheimer's disease, Trends Neurosci. 20 (1997) 154.

[4]D.J. Selkoe, Alzheimer's disease: genes, proteins, and therapy, Physiol Rev. 81 (2001) 741.

[5]D.J. Selkoe, Clearing the brain's amyloid cobwebs, Neuron 32 (2001) 177.

[6]S.G. Younkin, The role of Aβ42 in Alzheimer's disease, J Physiol Paris. 92 (1998) 289.

[7]A. Arora, C. Ha, C.B. Park, Inhibition of insulin amyloid formation by small stress molecules, FEBS Lett. 564 (2004) 121.

[8]B.J. Cummings, C.W. Cotman, Image analysis of β-amyloid load in Alzheimer's disease and relation to dementia severity, Lancet. 346 (1995) 1524.

[9]C. Haass, D.J. Selkoe, Soluble protein oligomers in neurodegeneration: lessons from the Alzheimer's amyloid β-peptide, Nat Rev Mol Cell Biol. 8 (2007) 101.

[10]A. Asami-Odaka, Y. Ishibashi, T. Kikuchi, C. Kitada, N. Suzuki, Long Amyloid. beta.-Protein Secreted from Wild-Type Human Neuroblastoma IMR-32 Cells, Biochem. 34 (1995) 10272.

[11]D. Schenk, R. Barbour, W. Dunn, G. Gordon, H. Grajeda, T. Guido, K. Hu, J. Huang, K. Johnson-Wood, K. Khan, Immunization with amyloid-β attenuates Alzheimer-disease-like pathology in the PDAPP mouse, Nature 400 (1999) 173.

[12]N. Andreasen, L. Minthon, P. Davidsson, E. Vanmechelen, H. Vanderstichele, B. Winblad, K. Blennow, Evaluation of CSF-tau and CSF-Aβ42 as diagnostic markers for Alzheimer disease in clinical practice, Arch Neurol. 58 (2001) 373.

[13]P. D. Mehta, T. Pirttilä, S.P. Mehta, E.A. Sersen, P.S. Aisen, H.M. Wisniewski, Plasma and cerebrospinal fluid levels of amyloid β proteins 1-40 and 1-42 in Alzheimer disease, Arch Neurol. 57 (2000) 100.

[14]D. Brambilla, R. Verpillot, M. Taverna, L. De Kimpe, B. Le Droumaguet, J. Nicolas, M. Canovi, M. Gobbi, F. Mantegazza, M. Salmona, New method based on capillary electrophoresis with laser-induced fluorescence detection (CE-LIF) to monitor interaction between nanoparticles and the amyloid-β peptide, Anal. Chem. 82 (2010) 10083.

[15]R. Wang, D. Sweeney, S.E. Gandy, S.S. Sisodia, The profile of soluble amyloid β protein in cultured cell media Detection and quantification of amyloid β protein and variants by immunoprecipitation-mass spectrometry, J. Biol. Chem. 271 (1996) 31894.

[16]G. Olivieri, C. Brack, F. Müller-Spahn, H. Stähelin, M. Herrmann, P. Renard, M. Brockhaus, C. Hock, Mercury Induces Cell Cytotoxicity and Oxidative Stress and Increases β-Amyloid Secretion and Tau Phosphorylation in SHSY5Y Neuroblastoma Cells, J. Neurochem. 74 (2000) 231.

[17]C.W. Cairo, A. Strzelec, R.M. Murphy, L.L. Kiessling, Affinity-based inhibition of β-amyloid toxicity, Biochem. 41 (2002) 8620.

[18]D.-Y. Kang, J.-H. Lee, B.-K. Oh, J.-W. Choi, Ultra-sensitive immunosensor for β-amyloid (1–42) using scanning tunneling microscopy-based electrical detection, Biosens. Bioelectron. 24 (2009) 1431.

[19]I.-H. Chou, M. Benford, H.T. Beier, G.L. Coté, M. Wang, N. Jing, J. Kameoka, T.A. Good, Nanofluidic biosensing for β-amyloid detection using surface enhanced

Raman spectroscopy, Nano Lett. 8 (2008) 1729.

[20]M.S. Shearman, D. Beher, E.E. Clarke, H.D. Lewis, T. Harrison, P. Hunt, A. Nadin, A.L. Smith, G. Stevenson, J.L. Castro, L-685,458, an aspartyl protease transition state mimic, is a potent inhibitor of amyloid β-protein precursor γ-secretase activity, Biochem. 39 (2000) 8698.

[21]J.A. Kotarek, K.C. Johnson, M.A. Moss, Quartz crystal microbalance analysis of growth kinetics for aggregation intermediates of the amyloid-β protein, Anal. Biochem. 378 (2008) 15.

[22]T.G. Drummond, M.G. Hill, J.K. Barton, Electrochemical DNA sensors, Nat. Biotechnol. 21 (2003) 1192.

[23]Y. Wang, C. Li, X. Li, Y. Li, H.-B. Kraatz, Unlabeled hairpin-DNA probe for the detection of single-nucleotide mismatches by electrochemical impedance spectroscopy, Anal. Chem. 80 (2008) 2255.

[24]J. Huang, G. Yang, W. Meng, L. Wu, A. Zhu, X.a. Jiao, An electrochemical impedimetric immunosensor for label-free detection of< i> Campylobacter jejuni</i> in diarrhea patients' stool based on O-carboxymethylchitosan surface modified Fe< sub> 3</sub> O< sub> 4</sub> nanoparticles, Biosens. Bioelectron. 25 (2010) 1204.

[25]J. Kafka, O. Pänke, B. Abendroth, F. Lisdat, A label-free DNA sensor based onimpedance spectroscopy, Electrochim. Acta. 53 (2008) 7467.

[26]J.S. Daniels, N. Pourmand, Label-Free Impedance Biosensors: Opportunities and Challenges, Electroanal. 19 (2007) 1239.

[27]M. Wang, L. Wang, G. Wang, X. Ji, Y. Bai, T. Li, S. Gong, J. Li, Application of impedance spectroscopy for monitoring colloid Au-enhanced antibody immobilization and antibody–antigen reactions, Biosens. Bioelectron. 19 (2004) 575.

[28]M.d. Vestergaard, K. Kerman, M. Saito, N. Nagatani, Y. Takamura, E. Tamiya, A rapid label-free electrochemical detection and kinetic study of Alzheimer's amyloid beta aggregation, J. Am. Chem. Soc. 127 (2005) 11892.

[29]K.Kerman, M.Chikae, S. Yamamura, E. Tamiya, Gold nanoparticle-based electrochemical detection of protein phosphorylation, Anal. Chim. Acta. 588 (2007) 26.

[30]I. Szymańska, H. Radecka, J. Radecki, R. Kaliszan, Electrochemical impedance spectroscopy for study of amyloid β-peptide interactions with (−) nicotine ditartrate and (−) cotinine, Biosens. Bioelectron. 22 (2007) 1955.

[31]M. Chikae, T. Fukuda, K. Kerman, K. Idegami, Y. Miura, E. Tamiya, Amyloid-β detection with saccharide immobilized gold nanoparticle on carbon electrode, Bioelectrochem. 74 (2008) 118.

[32]H. Li, Y. Cao, X. Wu, Z. Ye, G. Li, Peptide-based electrochemical biosensor for amyloid β 1–42 soluble oligomer assay, Talanta 93 (2012) 358.

[33]C.R. Lowe, Nanobiotechnology: the fabrication and applications of chemical and biological nanostructures, Curr. Opin. Struct. Biol. 10 (2000) 428.

[34]C.-C. Wu, P.-K. Tseng, C.-H. Tsai, Y.-L. Liu, Increased density and coverage uniformity of viruses on a sensor surface by using U-type, T-type, and W-type microfluidic devices, Biomicrofluidics 6 (2012) 024124.

[35]J.-J. Tsai, I.-J. Bau, H.-T. Chen, Y.-T. Lin, G.-J. Wang, A novel nanostructured biosensor for the detection of the dust mite antigen Der p2, Int. J. Nanomed. 6 (2011) 1201.

[36]Y.-S. Chen, G.-J. Wang, A high sensitivity and low-cost polycarbonate (PC)-based biosensor, Nano/Micro Engineered and Molecular Systems (NEMS), 2012 7th IEEE International Conference on, IEEE, 2012, pp. 392-397.

[37]Y.-F. Liu, J.-J. Tsai, Y.-T. Chin, E.-C. Liao, C.-C. Wu, G.-J. Wang, Detection of allergies using a silver nanoparticle modified nanostructured biosensor, Sens. Actuators, B 171 (2012) 1095.

[38]Y.-T. Chin, E.-C. Liao, C.-C. Wu, G.-J. Wang, J.-J. Tsai, Label-free detection of single-nucleotide polymorphisms associated with myeloid differentiation-2 using a nanostructured biosensor, Biosens. Bioelectron. 49 (2013) 506.

[39]J.A. Lee, S. Hwang, J. Kwak, S.I. Park, S.S. Lee, K.-C. Lee, An electrochemical impedance biosensor with aptamer-modified pyrolyzed carbon electrode for label-free protein detection, Sens. Actuators, B 129 (2008) 372.

[40]Y. Huang, M.C. Bell, I.I. Suni, Impedance biosensor for peanut protein Ara h 1, Anal. Chem. 80 (2008) 9157.

[41]A. Amirudin, D. Thieny, Application of electrochemical impedance spectroscopy to study the degradation of polymer-coated metals, Prog. Org. Coat. 26 (1995) 1.

[42]A. Parbhu, H. Lin, J. Thimm, R. Lal, Imaging real-time aggregation of amyloid beta protein (1–42) by atomic force microscopy, Peptides 23 (2002) 1265.

[43]W. Stine Jr, S. Snyder, U. Ladror, W. Wade, M. Miller, T. Perun, T. Holzman, G. Krafft, The nanometer-scale structure of amyloid-β visualized by atomic force microscopy, J. Protein Chem. 15 (1996) 193.

[44]R. BHATIA, H. Lin, R. LAL, Fresh and globular amyloid β protein (1–42) induces rapid cellular degeneration: evidence for AβP channel-mediated cellular toxicity, *FASEB J*. 14 (2000) 1233.

[45]D.T. Loo, A. Copani, C.J. Pike, E.R. Whittemore, A.J. Walencewicz, C.W. Cotman, Apoptosis is induced by beta-amyloid in cultured central nervous system neurons, Proc. Natl. Acad. Sci. U.S.A. 90 (1993) 7951.

Figure 1 Schematic illustration of the nanostructured biosensor

Figure 2 Immobilization of Aβ (1-42). (A) Deposition of gold nano particles on the surface of sensing electrode. The surface of the sensing electrode was washed by successively dipping it in acetone, ethanol, and DI water, followed by ultrasonic shaking for 5 min. (B) $10 \times 10^{-3}\ mol\ l^{-1}$ 20μL of a MUA solution was dipped onto the electrode surface. (C) 30 μL of a NHS and EDC solution with a molar ratio of 1:15 ($2 \times 10^{-3}\ mol\ l^{-1}$: $30 \times 10^{-3}\ mol\ l^{-1}$) in $15 \times 10^{-3}\ mol\ l^{-1}$ MES buffer was dipped onto the sensor and incubated for 1 hour. (D) 30 μL of a 10 μg ml^{-1} Aβ (1-42) antibody IgG solution was dipped onto the sensor and then incubating for 30 min. (E) The sensor was rinsed three times with a PBS buffer solution. The binding sites of the antigen molecules that did not bond with the MUA membrane were filled using 30 μL of a 7% BSA solution. (F) 30 μL of the A-beta(1-42) peptide solution was incubated onto the sensor for 30 minutes.

Figure 3 Western Blot analysis of Aβ (1-42) solution (A) Protein marker (B) GST-Aβ (1-42) solution from Abcam Inc.

Figure 4 SEM images of the (A) AAO barrier layer and (B) the GNP deposited nanostrucutred electrode

Figure 5 Cyclic voltammograms for three different electrodes (AAO/Au/GNP, AAO/Au film, and flat Au) in $5 \times 10^{-3}\ mol\ l^{-1}$ $Fe(CN)6^{4-}$, $5 \times 10^{-3}\ mol\ l^{-1}$ $Fe(CN)6^{3-}$, and 0.1 $mol\ l^{-1}$ in PBS buffer (A) I-V curve (B) I-t curve

Figure 6 Cyclic voltammograms of (A) MUA; (B) NHS/EDC; (C) antibody IgG; (D) BSA and (E) Aβ (1-42) immobilized electrode

Figure 7 Equivalent circuit for the nanostructured biosensor

Figure 8 The charge transfer resistances (R_{ct}) values with respect to corresponding antibody concentrations

Figure 9 SEM images (A) x3000 (B) x30000 of the substrate after modification with 1 μg ml^{-1} Aβ (1-42) for 30 min

Figure 10 AFM images of the substrate after modification with 1 μg ml^{-1} Aβ (1-42) peptides for 30 min

Figure 11 The impedance plots of (A) bare Au electrode; (B) MUA; (C) NHS/EDC; (D) IgG antibodies; (E) BSA and (F) with 100 pg ml^{-1} Aβ (1-42) immobilized electrode

Figure 12 The changes of R_{ct} values with respect to corresponding antigen concentrations

Table 1 XPS measurements for Au, C, O, S, N atom content ratio. We report also the water contact angle for characterized surface

Table 2 Cyclic voltammograms for the bare Au, MUA, IgG, BSA, and Aβ (1-42) immobilized electrodes

Table 3 The charge transfer resistances (R_{ct}) of different antibody concentrations

Table 4 Values of the circuit element from the experimental spectra after MUA, EDC/NHS, IgG, BSA and incubation of 100 pg ml^{-1} Aβ(1-42). The statistical values of mean $\pm$ standard deviation were calculated in five repetitions

Table 5 Values of ΔR_{ct} from the experimental spectra for different Aβ (1-42) peptide concentrations. The statistical values of mean $\pm$ standard deviation were calculated in five repetitions

Table 1 XPS measurements for Au, C, O, S, N atom content ratio. We report also the water contact angle for characterized surface

	Atomic composition / at%					Contact angle /。
Atom content ratio	Au	C	O	S	N	
(a)Uncoated	63.7	31.1	4.9	-	-	7.0
(b)MUA	15.1	67.1	17.3	0.5	-	67.7
(c)MUA and EDC/NHS	3.0	70.1	21.1	4.1	1.8	

Table 2 Cyclic voltammograms for the bare Au, MUA, IgG, BSA, and Aβ (1-42) immobilized electrodes

	MUA	EDC/NHS	IgG	BSA	Aβ(1-42)
ΔE_p / V	0.407	0.499	0.346	0.302	0.231

Table 3 The charge transfer resistance (R_{ct}) of different antibody concentrations

	Aβ(1-42) Antibody (1ng ml^{-1})	Aβ(1-42) Antibody (10ng ml^{-1})	Aβ(1-42) Antibody (100ng ml^{-1})	Aβ(1-42) Antibody (1μg ml^{-1})	Aβ(1-42) Antibody (10μg ml^{-1})
R_{ct} / kΩ	994	1234	1503	1583	1620

Table 4 Values of the circuit element from the experimental spectra after MUA, EDC/NHS, IgG, BSA and incubation of 100 pg ml^{-1} Aβ(1-42). The statistical values of mean ± standard deviation were calculated in five repetitions

	R_s / Ω	R_{nano} / kΩ	Q_s / nF	R_{ct} / kΩ	Q_{ct} / nF
MUA	41.3±0.2	9.3±0.2	2810.2±1.8	128.3±1.9	9231.2±1.1
EDC/NHS	38.7±1.2	8.8±0.9	2382.2±2.1	348.8±3.6	9140.5±0.7
IgG	39.5±2.1	9.0±1.1	2591.3±1.0	493.1±2.8	9126.8±0.6
BSA	40.3±0.1	8.8±0.3	2486.5±1.3	580.7±3.3	8952.7±0.8
Aβ(1-42)	40.0±0.8	8.9±0.4	2477.6±2.5	646.0±3.7	8793.9±0.5

Table 5 Values of ΔR_{ct} from the experimental spectra for different Aβ (1-42) peptide concentrations. The statistical values of mean ± standard deviation were calculated in five repetitions

	Aβ(1-42) (1pg ml^{-1})	Aβ(1-42) (10pg ml^{-1})	Aβ(1-42) (100pg ml^{-1})	Aβ(1-42) (10ng ml^{-1})
ΔR_{ct} / kΩ	85.48 ± 3.1	122.66 ± 2.90	152.71 ± 2.56	203.50 ± 4.27

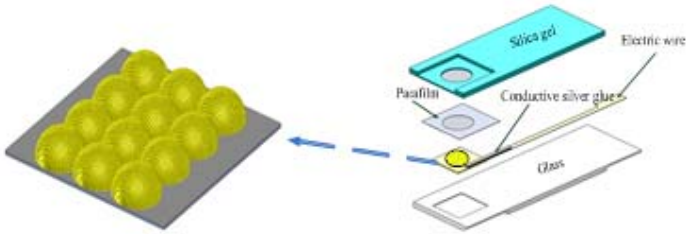

Figure 1 Schematic illustration of the nanostructured biosensor

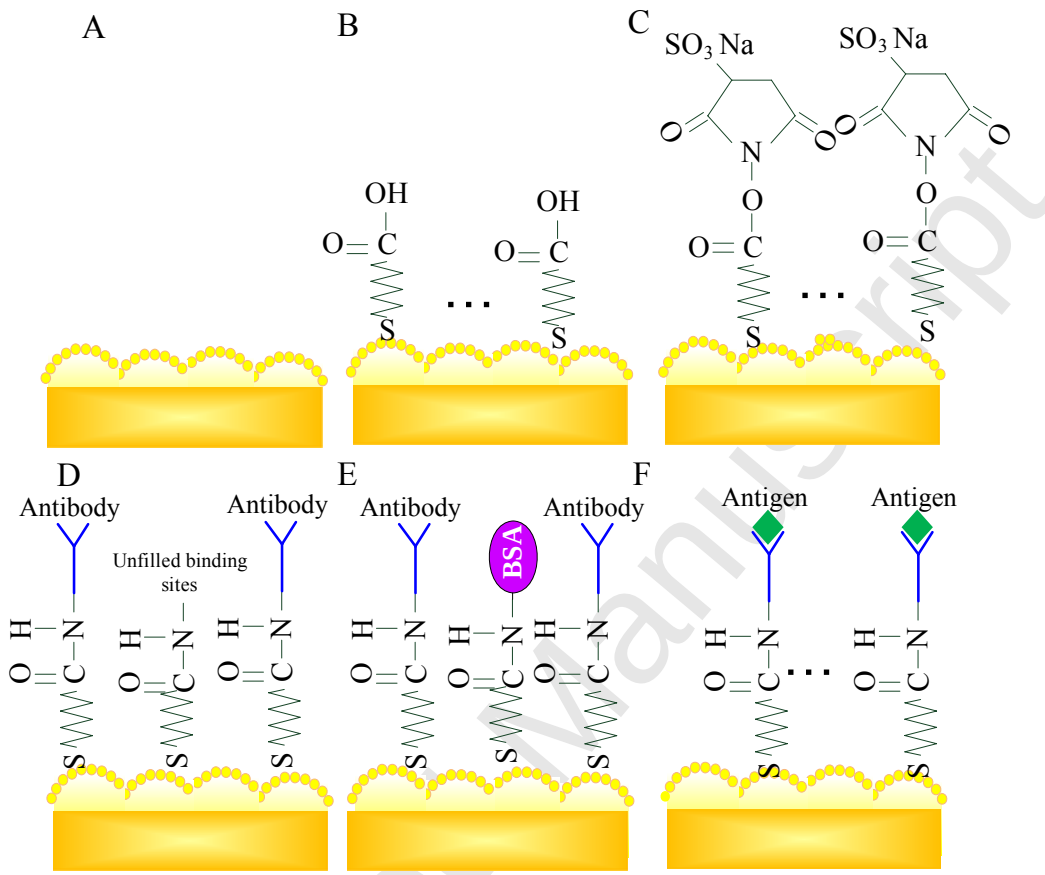

Figure 2 Immobilization of Aβ (1-42). (A) Deposition of gold nano particles on the surface of sensing electrode. The surface of the sensing electrode was washed by successively dipping it in acetone, ethanol, and DI water, followed by ultrasonic shaking for 5 min. (B) $10 \times 10^{-3}\ mol\ l^{-1}$ 20μL of a MUA solution was dipped onto the electrode surface. (C) 30 μL of a NHS and EDC solution with a molar ratio of 1:15 ($2 \times 10^{-3}\ mol\ l^{-1}$: $30 \times 10^{-3}\ mol\ l^{-1}$) in $15 \times 10^{-3}\ mol\ l^{-1}$ MES buffer was dipped onto the sensor and incubated for 1 hour. (D) 30 μL of a 10 μg ml^{-1} Aβ (1-42) antibody IgG solution was dipped onto the sensor and then incubating for 30 min. (E) The sensor was rinsed three times with a PBS buffer solution. The binding sites of the antigen molecules that did not bond with the MUA membrane were filled using 30 μL of a 7% BSA solution. (F) 30 μL of the A-beta(1-42) peptide solution was incubated onto the sensor for 30 minutes.

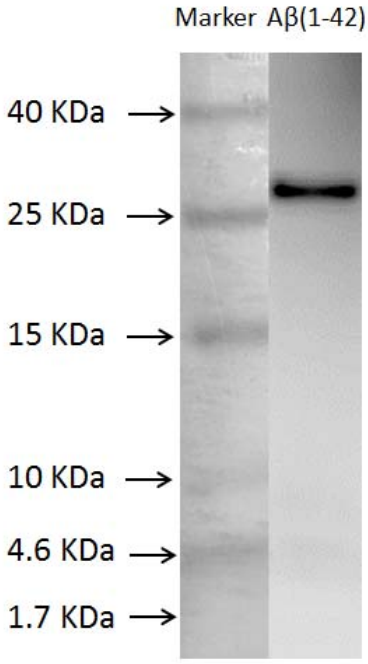

(A) (B)

Figure 3 Western Blot analysis of Aβ (1-42) solution (A) Protein marker (B) GST-Aβ (1-42) solution from Abcam Inc.

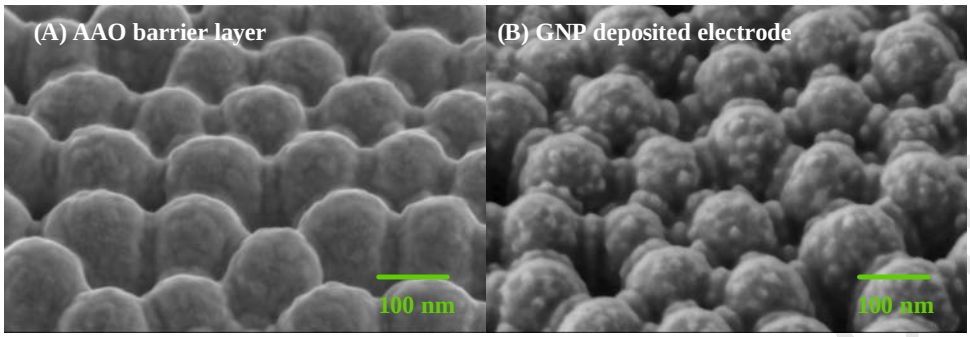

Figure 4 SEM images of the (A) AAO barrier layer and (B) the GNP deposited nanostrucutred electrode

A

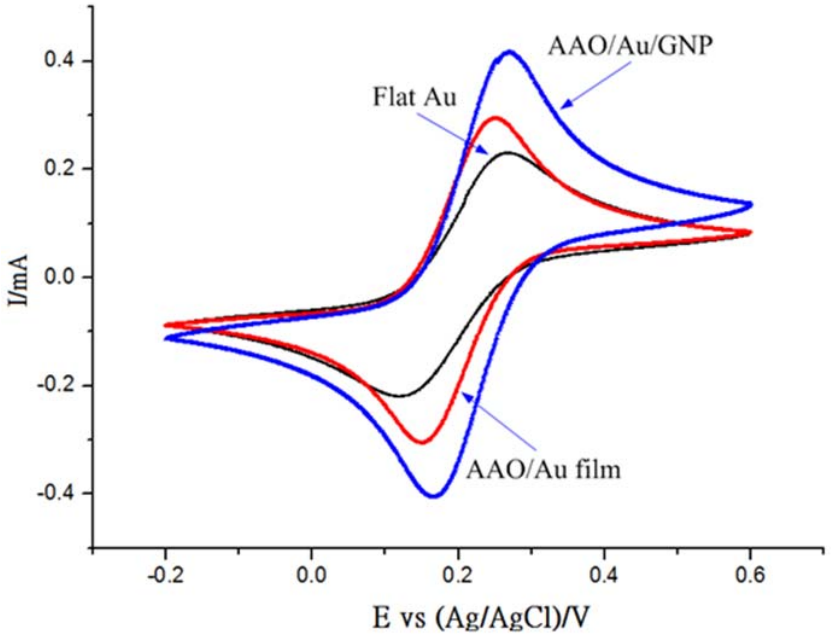

B

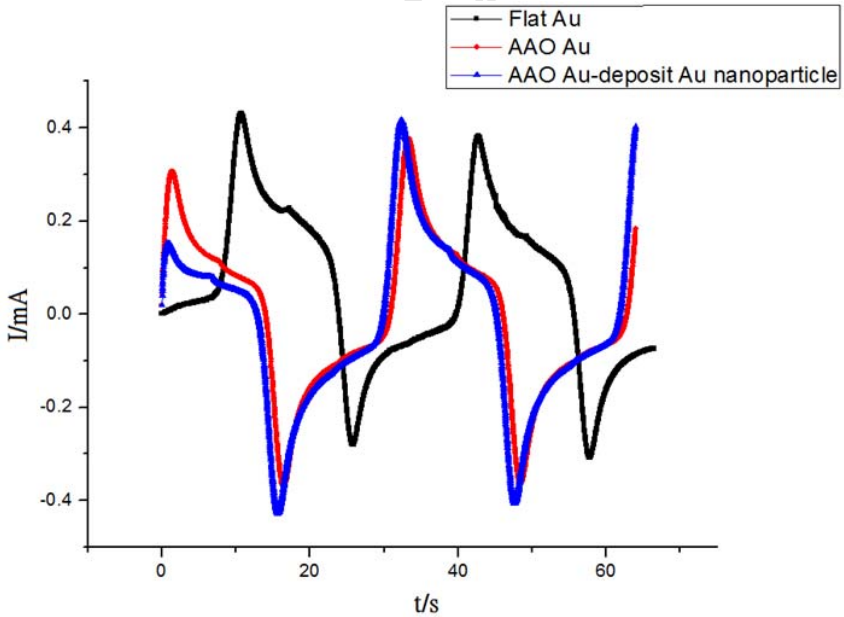

Figure 5 Cyclic voltammograms for three different electrodes

(A AO/Au/GNP, AAO/Au film, and flat Au) in 5×10^{-3} mol l^{-1} $Fe(CN)6^{4-}$, 5×10^{-3} mol l^{-1} $Fe(CN)6^{3-}$, and 0.1 mol l^{-1} in PBS buffer (A) I-V curve (B) I-t curve.

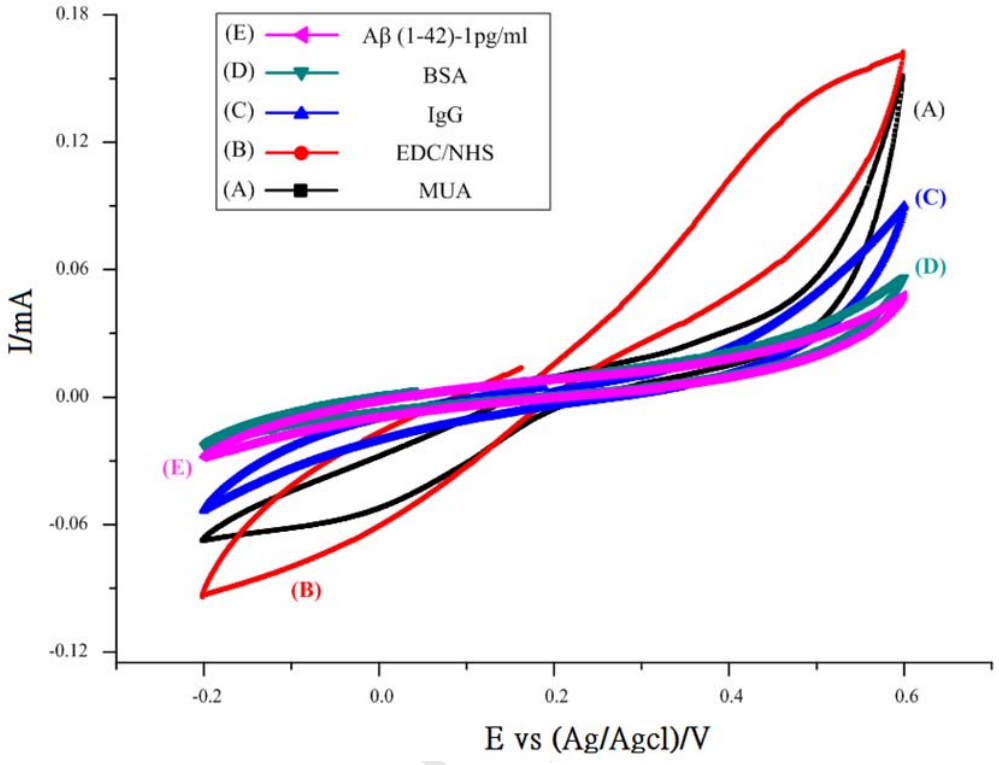

Figure 6 Cyclic voltammograms of (A) MUA; (B) NHS/EDC; (C) antibody IgG; (D) BSA and (E) Aβ (1-42) immobilized electrode

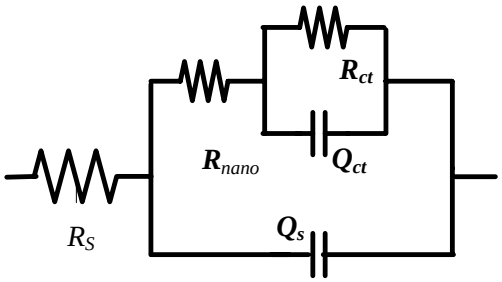

Figure 7 Equivalent circuit for the nanostructured biosensor

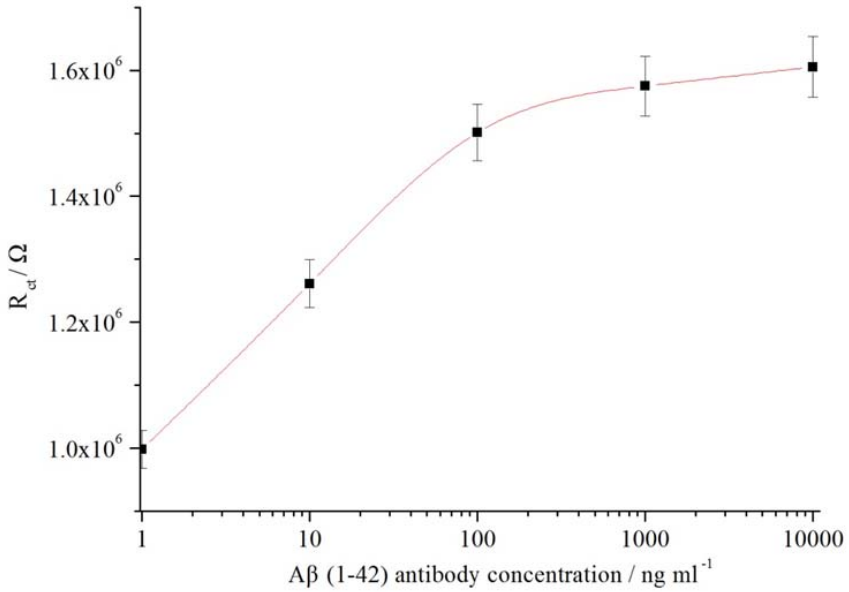

Figure 8 The charge transfer resistances (R_{ct}) values with respect to corresponding antibody concentrations

A **B**

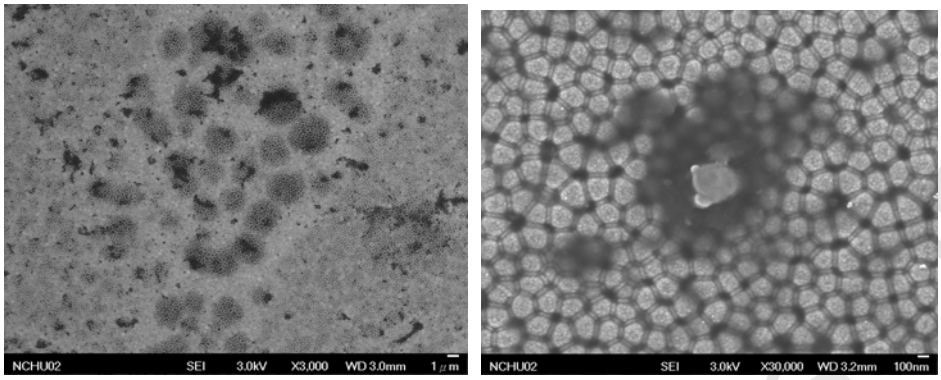

Figure 9 SEM images (A) x3000 (B) x30000 of the substrate after modification with 1 μg ml^{-1} Aβ (1-42) for 30 min

Figure 10 AFM images of the substrate after modification with 1 μg ml^{-1} Aβ (1-42) peptides for 30 min

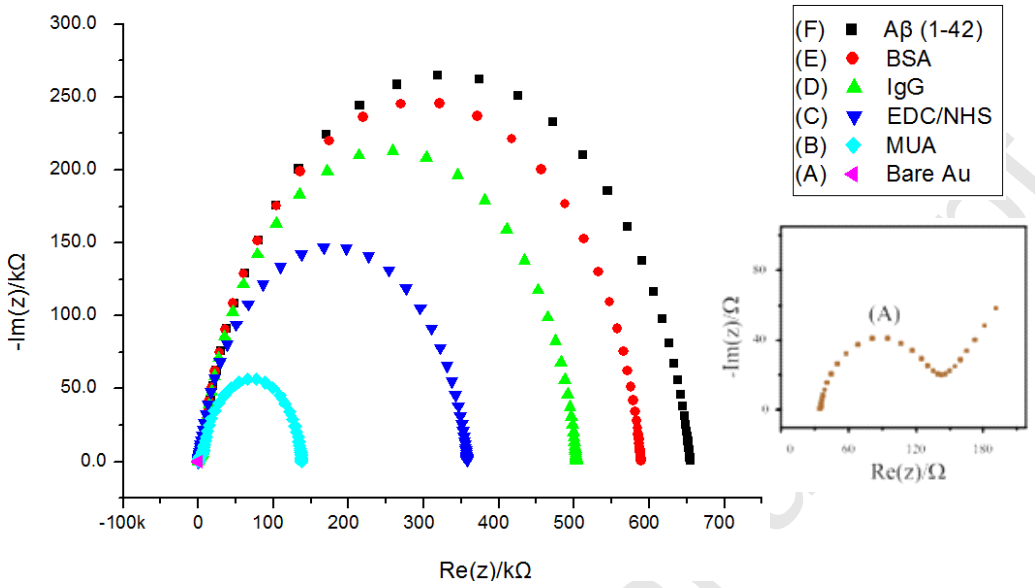

Figure 11 The impedance plots of (A) bare Au electrode; (B) MUA; (C) NHS/EDC; (D) IgG antibodies; (E) BSA and (F) with 100 pg ml^{-1} Aβ (1-42) immobilized electrode

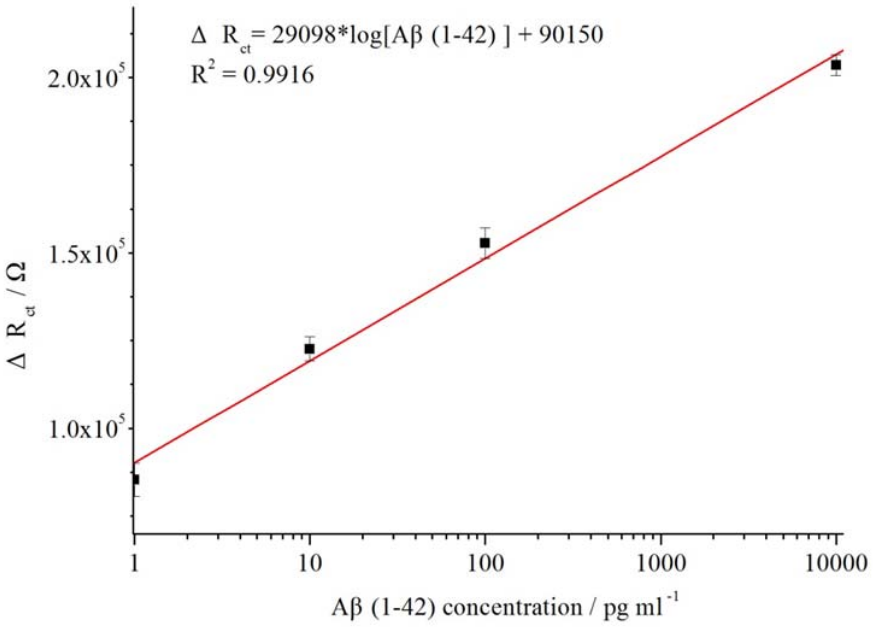

Figure 12 The changes of R_{ct} values with respect to corresponding antigen concentrations